Journal of Sound and Vibration (2000) **238**(4), 637–660
doi:10.1006/jsvi.2000.3088, available online at http://www.idealibrary.com on IDEAL®

SOUND FIELDS IN A SLIGHTLY DAMPED RECTANGULAR ENCLOSURE UNDER ACTIVE CONTROL

S. K. LAU AND S. K. TANG

Department of Building Services Engineering, The Hong Kong Polytechnic University, Hung Hom, Hong Kong, Peoples Republic of China. E-mail: besktang@polyu.edu.hk

(*Received* 12 *July* 1999, *and in final form* 12 *May* 2000)

Effectiveness of the global sound field control inside a slightly damped rectangular enclosure by using the potential energy, the squared pressure and the energy density as the cost function is investigated numerically in the present study. A detailed comparison between results obtained using pressure-squared sensing and energy density sensing is presented and the distributions of the zones of quiet are discussed. Three-dimensional visualization of the sound fields confirms that significant localized sound attenuation can be achieved in specific areas even an overall amplification of total potential energy in the enclosure results. The present results also show the occurrence of the detrimental effects and spillovers under the pressure-squared sensing, while they can be removed by using the energy density control. The energy density control results in more uniform sound fields, but is not effective if the error sensor is located between the primary and secondary sound sources. The present finding on producing large quiet zones using a simple system has significant implication for building noise control.

1. INTRODUCTION

Building services equipment is a major source of noise inside buildings. While the structure-borne sound may be reduced by an appropriate vibration isolation design, the low-frequency noise remains a problem, especially to the people staying in adjacent rooms or working in a control room inside/next to the plantroom. The technique of active noise control (ANC) [1] is expected to be a promising solution to this problem.

Two main categories of ANC strategies have been proposed for use in an enclosed space. They are the global and the local controls. The former concerns the attenuation of sound pressure at all points inside an enclosure [2, 3] whilst the latter is aimed at creating a quiet zone inside the enclosure [4, 5]. Nelson *et al.* [3] developed a theory for global control in an enclosure by minimizing the total time-averaged acoustic potential energy. This total acoustic potential energy, PE, is defined as

$$PE = \frac{1}{4\rho c^2} \int_V |p|^2 \, \mathrm{d}V, \tag{1}$$

where ρ is the air density, c the speed of sound, V the volume of the enclosure and p the sound pressure. Though PE simply represents the total acoustical energy inside an enclosure and its minimization would directly imply a lowering of the average sound

0022-460X/00/490637 + 24 $35.00/0

pressure level within the whole enclosed space, the implementation of this control in reality is difficult as a large number of sound pressure sensors are required.

The traditional squared-pressure control algorithm for ANC cannot produce a global sound reduction due to the limitation of local information, but it does produce a quiet zone in a confined small area inside an enclosed space. Elliott *et al.* [6] observed that a quiet zone can be formed within a diameter of about one-tenth of the acoustic wavelength around the error sensor in a fully diffused near sound field, within which at least 10 dB attenuation in sound pressure level can be achieved. Joseph *et al.* [4] found that this 10 dB quiet zone can be enlarged by increasing the separation between the secondary control source and error microphone. They also found that there is negligible increase in the sound pressure level far from this 10 dB quiet zone if the point of cancellation is very close to the secondary source. However, it may not be the case for a non-diffused sound field.

Recently, the energy density control algorithm was developed in the hope that a more effective global sound field control can be achieved [7–9]. The energy density, ED, is a local variable that sums up the acoustic potential energy density and kinetic energy density at a selected point X:

$$ED = \frac{|p(X)|^2}{2\rho c^2} + \frac{\rho |u(X)|^2}{2}, \tag{2}$$

where $u(X)$ is the air particle velocity due to acoustics. ED provides a more global information to the controller. In the one-dimensional application, the performance of ANC under this control algorithm is less dependent on the error sensor position [8]. Qiu *et al.* [9] have shown that this ED control is also effective in the middle free field. So far, however, the assessment of global control is only done in terms of the total potential energy PE reduction. There may then be a problem that the minimization of the total acoustic potential energy is done at the expense of sound pressure amplifications at some locations.

Apart from the control algorithm, another important issue in the design of a physical ANC system is to lay the error sensors and the secondary control sources in the best positions according to the primary noise characteristics. Some strategies for the selection of optimal placement of error sensors and secondary sources have been proposed in recent years as reviewed, for instance, by Hansen and Synder [10]. Natural algorithms [11] such as the genetic algorithms [12] and the simulated annealing algorithms [13] are useful for locating the secondary control sources, while the multiple regression method is proposed by Synder and Hansen [14, 15] for optimizing the position of error sensor. Nelson and Elliott [16] and Maa [17] proposed to locate the error sensor at a corner for global control of low-frequency sound using the squared-pressure method. However, the actual sound field and the distribution of quiet zones under this corner ANC are not well documented. The performance of this system under the energy density sensing has not been explored.

Though a global reduction of sound is ideal, it is not that important in building noise control in general as sound transmission or radiation may only relate to some particular parts inside an enclosure. It is the sound field pattern that really matters. In the present study, a detailed study on the sound field in a slightly damped rectangular enclosure under ANC implemented by using different cost functions, namely the potential energy, squared pressure and energy density, inside an enclosed space is carried out. Effects of error sensor locations are also examined. It is hoped that the present results can provide a clearer picture on the overall performance of the ANC inside enclosed space and give guidance for a more effective use of ANC in buildings. Since the noisy building services equipment are installed in the mechanical plantrooms, which are basically rectangular enclosures with limited sound absorption especially at low frequencies, the present study is focussed on the

application of ANC in a slightly damped rectangular enclosure. Practising engineers would not favour complicated internal geometry as it reduces the flexibility of equipment installation and space utilization, and may also make maintenance difficult. In noise control, it will result in higher modal density, making the prediction of sound field and the implementation of ANC difficult.

2. OPTIMIZATION OF SECONDARY SOURCE STRENGTHS

Sound field inside an enclosure can be found by the summation of infinite sets of modal components. The sound pressure at any point $X(x, y, z)$ inside the enclosed space due to steady primary and secondary sound sources in the ANC system can be determined by the following modal equation as in Park and Sommerfeldt [8]:

$$p(X) = \sum_{n=0}^{\infty} (A_n + B_n Q_s) \Phi_n(X), \tag{3}$$

where A_n and B_n are the modal weights for the primary and secondary sound fields, respectively, Φ_n represents the nth eigenfunction of the acoustic modal pressure distribution inside the enclosed space and Q_s is the secondary source strength.

The optimal secondary source strength, Q_s, depends on the locations of the error sensor, primary source and secondary source (hereinafter denoted by X_e, X_p and X_s respectively). It is also related to the strength of primary sources and the choice of the cost function. In the foregoing discussions, suffices PE, SP and ED denote quantities associated with the potential energy, squared-pressure and energy density control algorithms respectively. The theoretical solutions of optimized secondary sound source strengths to minimize the cost functions can be expressed respectively as [8]

$$Q_{s,PE} = -\sum_{n=0}^{\infty} B_n^* A_n \Big/ \sum_{n=0}^{\infty} B_n^* B_n, \tag{4}$$

$$Q_{s,SP} = -\sum_{n=0}^{\infty} A_n \Phi_n(X_e) \Big/ \sum_{n=0}^{\infty} B_n \Phi_n(X_e), \tag{5}$$

$$Q_{s,ED} = -\sum_{m=0}^{\infty} \sum_{n=0}^{\infty} A_m B_n^* F_{m,n}(X_e) \Big/ \sum_{m=0}^{\infty} \sum_{n=0}^{\infty} B_m B_n^* F_{m,n}(X_e), \tag{6}$$

where

$$F_{m,n}(X_e) = \Phi_m(X_e) \Phi_n(X_e) + \frac{1}{k^2} \nabla \Phi_m(X_e) \nabla \Phi_n(X_e), \tag{7}$$

k is the acoustic wave number and * denotes the complex conjugate. The subscripts m and n are the mode numbers. The sound pressure throughout the enclosed space can be found by equation (3) with the optimized source strengths depicted in equations (4)–(6). Though infinite number of modes are contributing to the enclosed sound field, only a finite number of them are practically important in the calculation as far as engineering accuracy is concerned. The choice of this number will be discussed in the next section. A formal derivation for equation (4)–(6) can be found in Park and Sommerfeldt [8].

3. NUMERICAL MODEL AND CONVERGENCE

The rectangular enclosure and the co-ordinate system adopted in the present study are illustrated in Figure 1. We chose its dimensions L_x (length), L_y (width) and L_z (height) in such a way that $L_x : L_y : L_z = 1 : e/\pi : 1/\pi$, where e denotes the exponential constant, in order to avoid the degenerate modes as in Joseph *et al.* [18]. The secondary sound source S_s was located at a corner throughout the numerical experiment. S_p represents the primary noise source, which was located either at $(0{\cdot}5L_x, 0{\cdot}5L_y, 0{\cdot}5L_z)$ or $(0{\cdot}25L_x, 0{\cdot}5L_y, 0{\cdot}5L_z)$ in the present investigation. This is a typical situation found in a plantroom where the noisy machine (primary noise source) is usually located sufficiently far away from the walls or near to the centre of the room in order to maintain a reasonable degree of accessibility for future maintenance or modification.

All frequencies in the foregoing discussions are normalized by the first cut-off frequency, f_c, which corresponds to the (1, 0, 0) mode frequency. Joseph *et al.* [18] have found, using a statistical approach, that ANC is effective for minimizing the total potential energy if the average level of modal overlap is less than 0·3. A modal overlap of 0·3 corresponds to an upper frequency limit of $2{\cdot}8f_c$ ($\sim 3f_c$) in the present study. The modal weights in equation (3) were obtained by using the method of Nelson *et al.* [3] with a modal damping coefficient of 0·01. All the simulations were computed by using MATLAB on a DEC workstation 600 a.u.

To calculate the sound field, equation (3) requires the summation of an infinite number of modes. However, as mentioned before, only a finite number of modes are practically important for this purpose. Therefore, a convergence test was done in the first place. In the test, we chose a frequency of $3f_c$ and S_p was located at $(0{\cdot}5L_x, 0{\cdot}5L_y, 0{\cdot}5L_z)$. Though there is an inherent convergence difficulty of equation (3) close to or at the sound source [19], it is

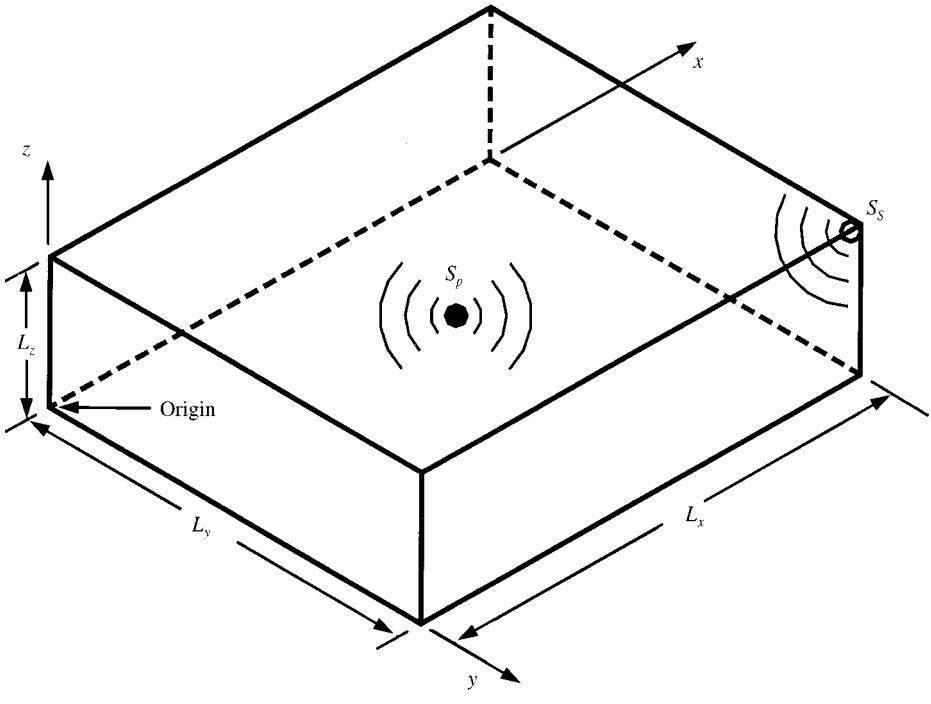

Figure 1. Rectangular enclosed space and co-ordinate system.

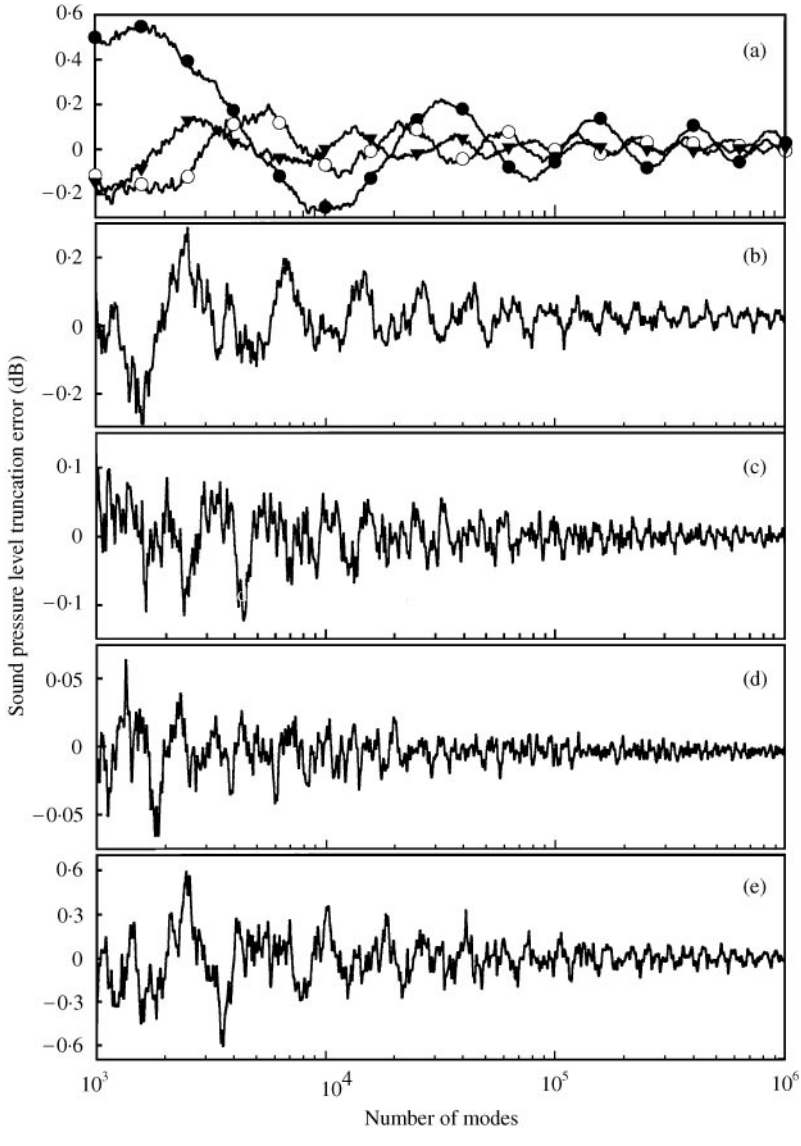

Figure 2. Convergence of modal summation at different locations with a point source at $(0{\cdot}5L_x, 0{\cdot}5L_y, 0{\cdot}5L_z)$: (a) –●– $(0{\cdot}45L_x, 0{\cdot}5L_y, 0{\cdot}5L_z)$; –○– $(0{\cdot}5L_x, 0{\cdot}45L_y, 0{\cdot}5L_z)$ and –▼– $(0{\cdot}5L_x, 0{\cdot}5L_y, 0{\cdot}35L_z)$; (b) $(0{\cdot}3L_x, 0{\cdot}5L_y, 0{\cdot}5L_z)$; (c) $(0{\cdot}2L_x, 0{\cdot}5L_y, 0{\cdot}5L_z)$; (d) $(0{\cdot}1L_x, 0{\cdot}5L_y, 0{\cdot}5L_z)$; (e) $(0{\cdot}25L_x, 0{\cdot}5L_y, 0{\cdot}5L_z)$

not worthwhile to study the sound pressure at those points. Figure 2(a) shows the convergence of the nearfield sound pressure level calculated by using equation (3) at $3f_c$ at a location 7·5% of the wavelength from S_p. The maximum deviations from the result obtained after summing up the effects of the first 1 035 974 modes are less than 0·5, 0·3 and 0·2 dB for summations over the first 2000, 9000 and 20 000 modes respectively. Figures 2(b)–2(d) show the corresponding results at various locations within the enclosure. Faster convergence can be found at increased distance away from the primary sound source. The convergence of sound pressure level at one of the nodal points is shown in

Figure 2(e). The truncation error is less than 0·4 dB if the contributions from the first 9000 modes were included.

Study has been extended to other points along the y and z directions as well as putting S_p at the corner. Basically, similar or even better convergence than that shown in Figure 2 is found except at the anti-nodes of the (1, 0, 0) mode and thus the associated results are not presented. The number of modes in the calculation of the sound field was set to be 9000.

4. TOTAL ACOUSTIC POTENTIAL ENERGY

As mentioned previously, the total acoustic potential energy is a common measure to determine the global effectiveness of the control algorithms [3, 8]. For orthogonal modal characteristic functions, the integral of potential energy (equation (1)) gives

$$PE = \frac{V}{4\rho c^2} \sum_{n=0}^{\infty} |A_n + B_n Q_s|^2. \tag{8}$$

Figure 3 illustrates the attenuation of PE up to $3f_c$ when the error sensor was located near the diagonal line between the two ceiling corners $(0, 0, L_z)$ and (L_x, L_y, L_z), while S_p and S_s were fixed at $(0{\cdot}5L_x, 0{\cdot}5L_y, 0{\cdot}5L_z)$ and (L_x, L_y, L_z) respectively. The calculations were done at $0{\cdot}02f_c$ intervals. Also, the attenuation greater than ± 30 dB was truncated. Table 1 shows the frequencies of the first eight eigenmodes.

In general, the potential energy control algorithm provides a relatively higher attenuation of the total acoustic potential energy at very low frequencies ($<0{\cdot}8f_c$) and at around $2f_c$. However, no attenuation is found between f_c and $1{\cdot}5f_c$. There are two reasons for this. The first reason is that the centre primary source falls onto the nodal planes of the (1, 0, 0), (0, 1, 0) and (1, 1, 0) modes having frequencies of f_c, $1{\cdot}16f_c$ and $1{\cdot}53f_c$, respectively, as explained in Nelson and Elliott [16]. These frequencies are hereinafter referred to as the uncontrollable eigenfrequencies. The second is due to the small Q_s that resulted from the vanishing A_ns on the nodal planes at these frequencies (equations (4)–(6)). A sharp attenuation of potential energy is also observed at frequencies higher than $3f_c$. However, the magnitude of such attenuation becomes much lower. Thus, effective global reduction of sound level through the potential energy control algorithm is limited to a frequency less than the first cut-off frequency if the total acoustic potential energy is concerned. It is consistent with the conclusion of Nelson and Elliott [16] that the amplitudes of a specified number of modes can be independently and effectively controlled by the same number of secondary sources.

Minimizing squared pressure at the error sensor location gives basically similar SPL attenuation at around $2f_c$ as in the potential energy control. However, detrimental effects at frequencies between the room modes or near the frequency $2f_c$ occur when the error sensor is located near to the secondary source as shown in Figures 3(a) and 3(b) (detrimental effects occur at $2{\cdot}06f_c$ in these figures). Spillovers exist at some eigenfrequencies greater than f_c. The first detrimental effect occurs at $0{\cdot}3f_c$ when the error sensor is located at $(0{\cdot}9L_x, 0{\cdot}9L_y, 0{\cdot}9L_z)$, which is a position near to the corner secondary source (Figure 3(a)). The frequency at which the first detrimental effect occurs gradually shifts toward f_c as the error sensor is being moved away from the corner secondary source to the location above the primary source as shown in Figures 3(b) and 3(c). For all cases investigated in the present study, it is found that the closer the error sensor to the corner secondary source, the smaller this frequency will be. The detrimental effect at low frequency becomes much

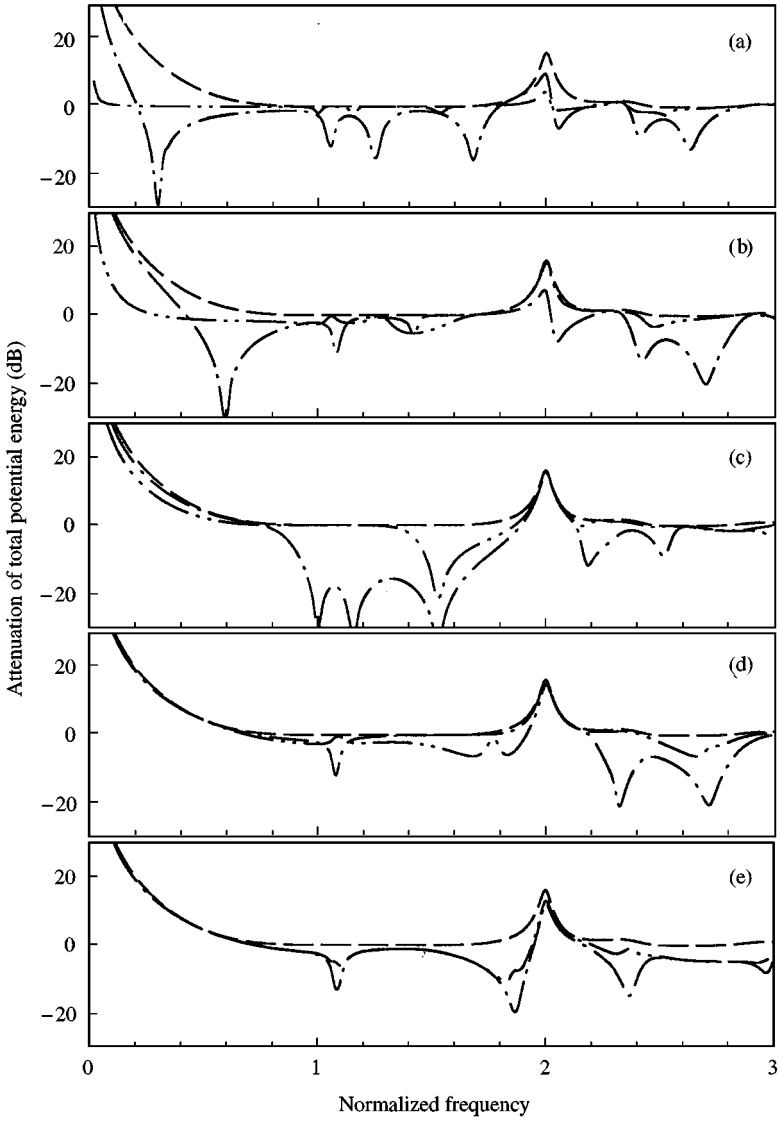

Figure 3. Variation of total acoustic potential energy attenuation with frequency for primary source at $(0{\cdot}5L_x, 0{\cdot}5L_y, 0{\cdot}5L_z)$ under different error sensor locations. (a) $(0{\cdot}9L_x, 0{\cdot}9L_y, 0{\cdot}9L_z)$; (b) $(0{\cdot}7L_x, 0{\cdot}7L_y, 0{\cdot}9L_z)$; (c) $(0{\cdot}5L_x, 0{\cdot}5L_y, 0{\cdot}9L_z)$; (d) $(0{\cdot}3L_x, 0{\cdot}3L_y, 0{\cdot}9L_z)$; (e) $(0{\cdot}1L_x, 0{\cdot}1L_y, 0{\cdot}9L_z)$: ——, potential energy control; — — —, squared pressure control; — — — —, energy density control. Secondary source at (L_x, L_y, L_z).

less important when the error sensor is located further away from the secondary sound source.

The above-mentioned detrimental effect results from the small secondary sound field near to the error sensor, so that an abnormally large secondary source strength is required to control the primary sound field, especially at low frequency. The enclosed sound field is not uniform even though the frequency is very low. The required secondary source strength for the squared-pressure control can be determined by equation (5). Denoting $\mathrm{j} = \sqrt{-1}$, it can be shown that the denominator of equation (5) is the normalized sound pressure at the error

TABLE 1

Normalized eigenfrequency of the enclosure

Modes	Normalized natural frequency
(1, 0, 0)	1·00
(0, 1, 0)	1·16
(1, 1, 0)	1·53
(2, 0, 0)	2·00
(2, 1, 0)	2·31
(0, 2, 0)	2·31
(1, 2, 0)	2·52
(3, 0, 0)	3·00

sensor location by that due to the secondary source alone:

$$\begin{aligned}\frac{V}{\rho c^2}\frac{P_s(X_e)}{Q_{s,SP}} &= \sum_{n=0}^{\infty} B_n \Phi_n(X_e)\\ &= \sum_{n=0}^{\infty} \frac{\omega}{2\xi_n\omega_n\omega - \mathrm{j}(\omega_n^2 - \omega^2)}\,\Phi_n(X_s)\Phi_n(X_e)\\ &= \sum_{n=0}^{\infty} \frac{2\xi_n\omega_n\omega^2}{(2\xi_n\omega_n\omega)^2 + (\omega_n^2 - \omega^2)^2}\,\Phi_n(X_s)\Phi_n(X_e)\\ &\quad + \mathrm{j}\sum_{n=0}^{\infty} \frac{\omega(\omega_n^2 - \omega^2)}{(2\xi_n\omega_n\omega)^2 + (\omega_n^2 - \omega^2)^2}\,\Phi_n(X_s)\Phi_n(X_e),\end{aligned} \tag{9}$$

where $P_s(X_e)$, ξ_n, ω, ω_n and $\Phi_n(X_s)$ are the sound pressure at error sensor location due to the secondary source only, damping coefficient, angular frequency of sound, natural frequency of the enclosure and eigenfunctions of the acoustic modal pressure distribution (real) respectively. When the secondary source and error sensor are close to a corner, the product of the eigenfunctions $\Phi_n(X_s)\Phi_n(X_e)$ in equation (9) is always positive for all n. Each element of the real part of equation (9) is small and positive, and so is the resultant real part. However, the imaginary part of equation (9) contains negative and positive elements for $\omega_n < \omega$ and $\omega_n > \omega$ respectively. At the frequency of the occurrence of the detrimental effect, the sum of these negative and positive imaginary elements is nearly zero and thus $Q_{s,SP}$ of equation (5) is large as $P_s(X_e)$ is, in general, finite.

Figure 4(a) and 4(b) illustrate the sound field at the level of error sensor ($z = 0{\cdot}9L_z$) due to the secondary source only at the frequency $0{\cdot}3f_c$ and $0{\cdot}6f_c$ respectively. The source strengths in Figure 4 are $V/\rho c^2$. Small sound pressures are observed at the points of error sensors due to the vanishing imaginary part of equation (9). A remote error sensor can thus eliminate the detrimental effect due to the eigenfunction products $\Phi_n(X_s)\Phi_n(X_e)$ that tend to avoid a vanishing imaginary part.

It will be shown later in section 5 that at the frequency of occurrence of the detrimental effect, sound pressures throughout the enclosed space, except at the error sensor location, are largely amplified, especially at frequencies below f_c. Placing the error sensor behind the primary centre source near to the opposite corner of the secondary corner source can eliminate the detrimental effect below f_c (Figures 3(d) and 3(e)), but the detrimental effects

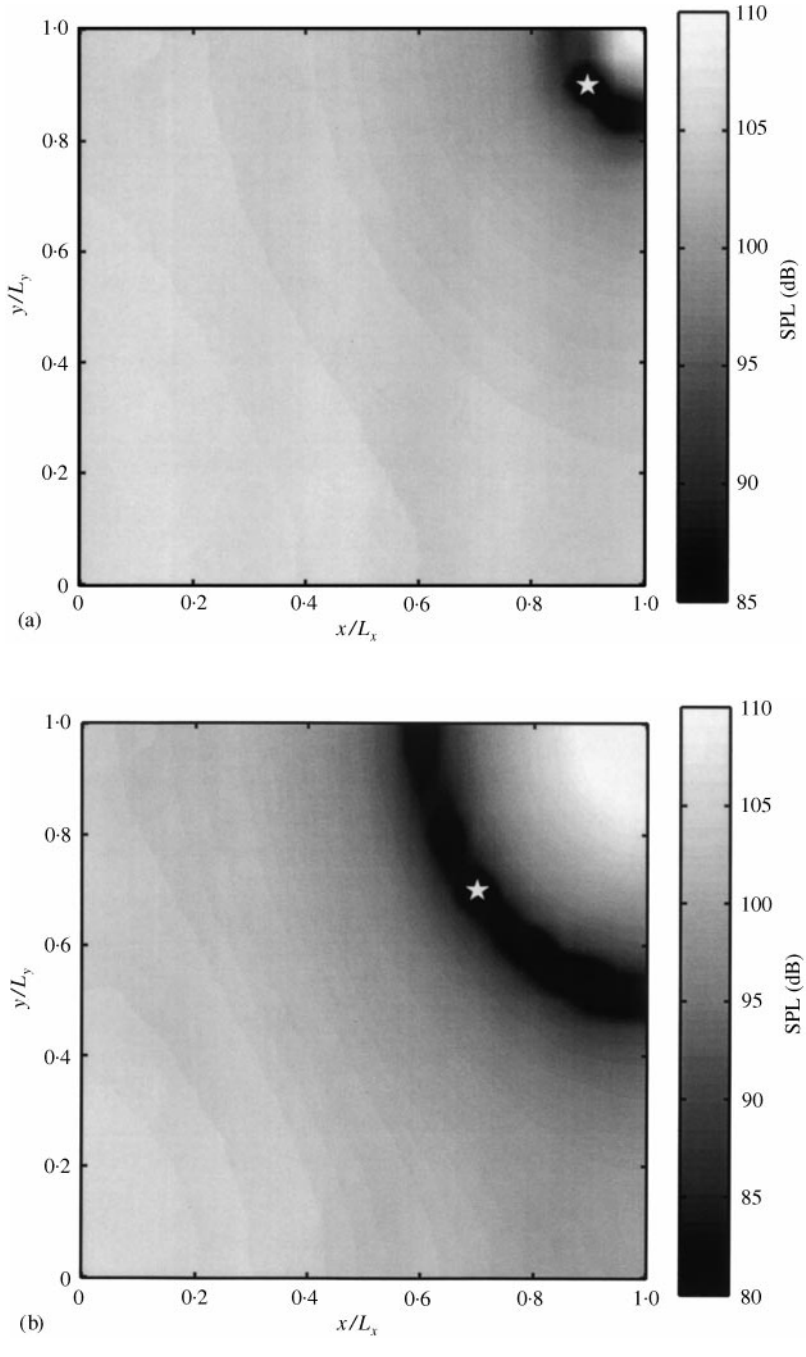

Figure 4. Map of sound pressure level (dB) due solely to secondary corner source: (a) $0{\cdot}3f_c$; error sensor at $(0{\cdot}9L_x, 0{\cdot}9L_y, 0{\cdot}9L_z)$; (b) $0{\cdot}6f_c$; error sensor at $(0{\cdot}7L_x, 0{\cdot}7L_y, 0{\cdot}9L_z)$. $z = 0{\cdot}9L_z$; ☆, error sensor location.

and spillovers still exist at higher frequencies. The amplifications at f_c, $1{\cdot}15f_c$, $1{\cdot}53f_c$ and $2{\cdot}52f_c$ shown in Figure 3(c) are due to the spillovers of the (1, 0, 0), (0, 1, 0), (1, 1, 0) and (1, 2, 0) modes respectively. In Figure 3(d), the amplification at $2{\cdot}31f_c$ is due to the spillover of the (0, 2, 0) mode, while all the others in Figure 3 are due to the detrimental effects.

The energy density control algorithm results in much less significant detrimental effect and spillover than the squared-pressure algorithm, especially at frequencies below f_c for all the error sensor locations investigated (Figure 3). However, large spillover at the (1, 1, 0) mode is observed for both the energy density and squared-pressure algorithms at an error sensor position of $(0{\cdot}5L_x, 0{\cdot}5L_y, 0{\cdot}9L_z)$, suggesting that locations directly above S_p are not suitable for ANC. It is observed that the performance of the energy density algorithm becomes similar to that of the squared-pressure one as the error sensor is located towards the corner opposite to the secondary source (Figures 3(d) and 3(e)). When the error sensor is located closer to S_s, the secondary sound field tends to have no effect on the total potential energy for frequencies less that f_c. This is due to the non-uniform energy density field as explained in the next paragraph.

Defining the energy density of secondary source, ED_s, and the correlative energy density between the primary and secondary sources, ED_c, at the error sensor, position X_e as

$$ED_s = \frac{1}{2\rho c^2} \sum_{m=0}^{\infty} \sum_{n=0}^{\infty} B_m B_n^* F_{m,n}(X_e) \tag{10a}$$

and

$$ED_c = \frac{1}{2\rho c^2} \sum_{m=0}^{\infty} \sum_{n=0}^{\infty} A_m B_n^* F_{m,n}(X_e), \tag{10b}$$

respectively, it can be observed from equation (6) that the optimized secondary source strength under the energy density control depends on the ratio ED_c/ED_s.

Figure 5(a) shows the map of ED_s at the level of the error sensor ($z = 0{\cdot}9L_z$) at $0{\cdot}3f_c$. The energy density is high and non-uniform around the secondary source. The same phenomenon occurs when only the primary source is operating (not shown here). The corresponding ED_c between the two sources is also non-uniform and small (Figures 5(b)). The small optimal secondary source strength so produced is due to the small ED_c and/or the large ED_s at the location of error sensor (equation (6)). The performance of ANC in this circumstance depends very critically on the error sensor location. This phenomenon can be avoided by remote-error sensing.

Figure 6 shows the attenuation of the total acoustic potential energy when S_p is located closer to one of the walls at $(0{\cdot}25L_x, 0{\cdot}5L_y, 0{\cdot}5L_z)$. The positions of S_s and the error sensor are the same as those in Figure 3. High attenuation of total potential energy is observed at low frequencies and at around f_c. ANC is not effective between $1{\cdot}2f_c$ and $2{\cdot}3f_c$ because the primary source S_p falls onto the nodal planes of the (0, 1, 0) (1, 1, 0) (2, 0, 0) and (2, 1, 0) modes. For frequencies less than f_c, similar detrimental effects as in the squared-pressure control cases (Figures 3(a) and 3(b)) occur again at frequencies of $0{\cdot}3f_c$ and $0{\cdot}6f_c$ as illustrated in Figures 6(a) and 6(b), respectively, when the error sensor is located near to the secondary source. The energy density algorithm produces approximately the same effects on the attenuation of the total potential energy as the potential energy algorithm except when the error sensor is not located between the two sound sources.

It can be observed from Figures 3 and 6 that the margins of attenuation of the total potential energy for the three control algorithms are narrow for frequency above the first cut-off frequency. However, it is possible that the "quiet zones" and "amplification zones" may co-exist inside the enclosure under ANC so that a reduction in the total potential energy does not necessarily imply the reduction of sound pressure level throughout the enclosure. Also, the sound field under ANC inside an enclosure is expected to be non-uniform so that the occurrence of the detrimental effects and spillovers in the total

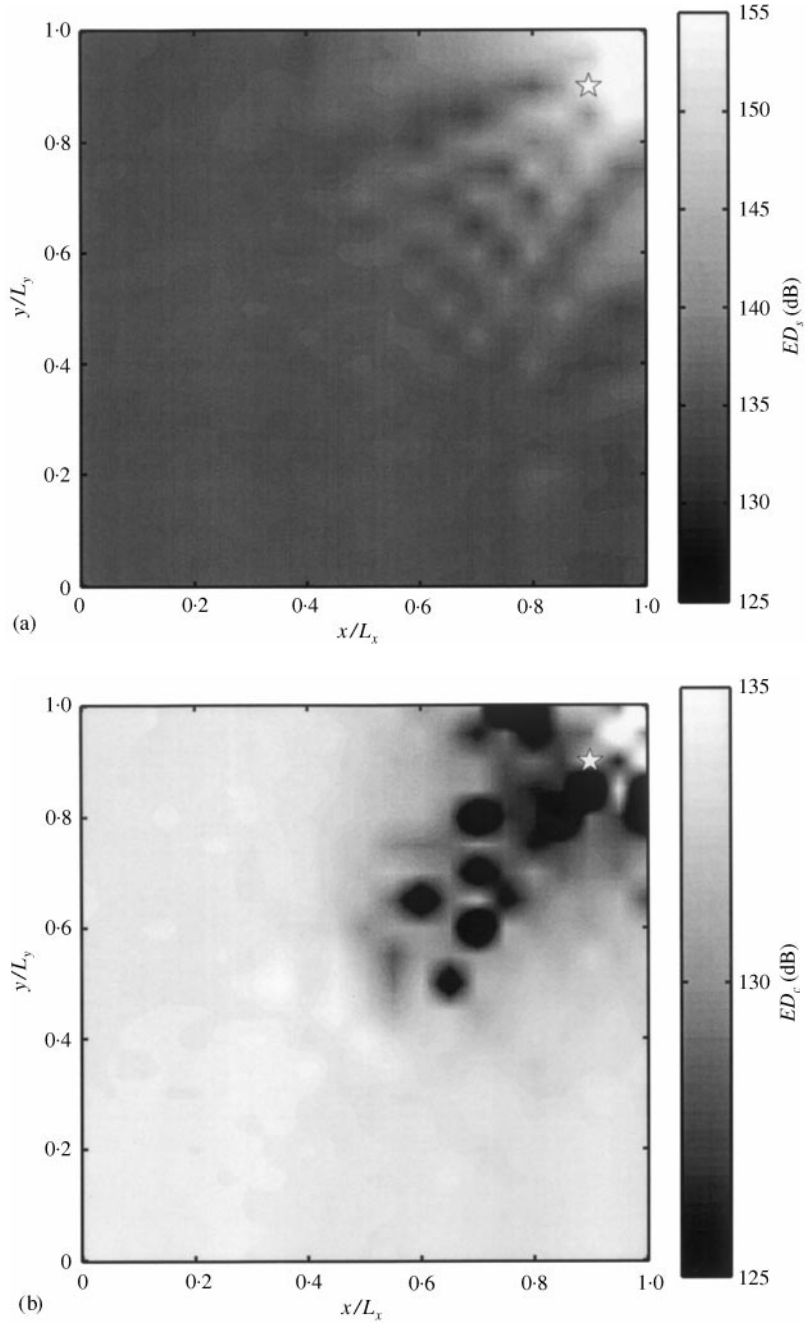

Figure 5. (a) Energy density map due solely to secondary corner source; (b) Correlative energy density map. $z = 0{\cdot}9L_z$. Frequency $= 0{\cdot}3f_c$. Error sensor, ☆, at $(0{\cdot}9L_x, 0{\cdot}9L_y, 0{\cdot}9L_z)$. All data presented are in dB ref. 10^{-12} N/m^2.

potential energy data may not be totally unacceptable. The discussions on the applicability of ANC and the effectiveness of the control algorithms require an understanding of the actual sound field. This will be discussed in the next section.

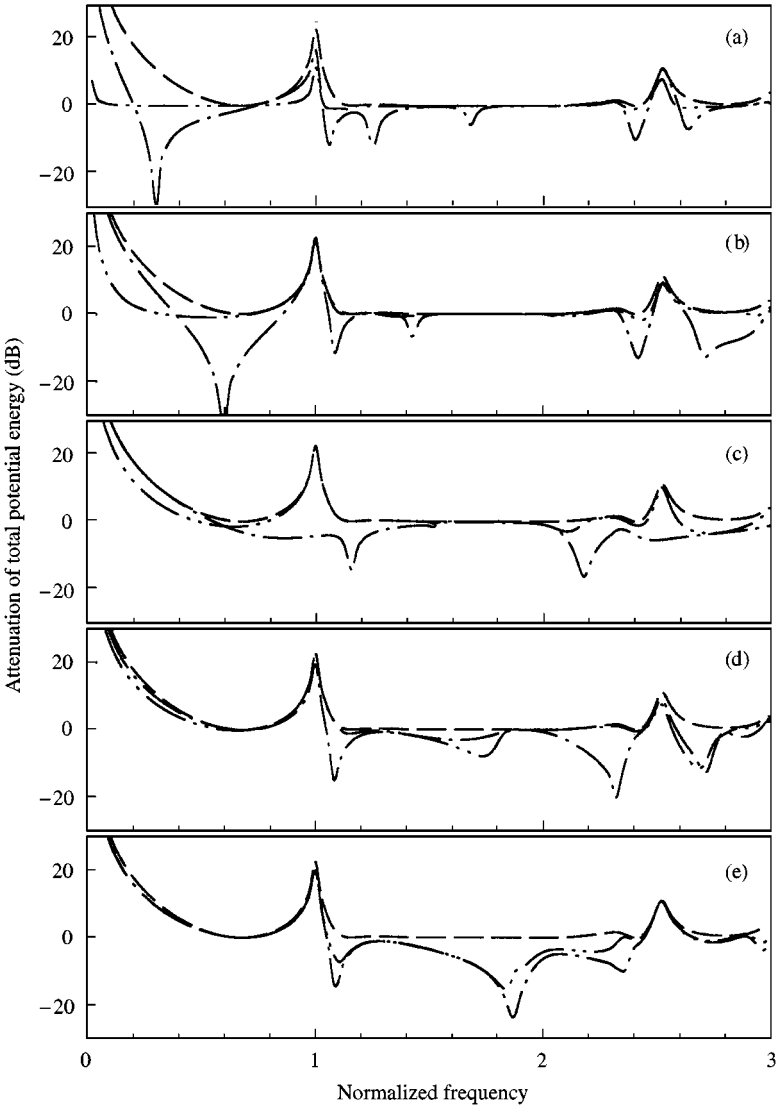

Figure 6. Variation of total acoustic potential energy attenuation with frequency for primary source at $(0{\cdot}25L_x, 0{\cdot}5L_y, 0{\cdot}5L_z)$ under different error sensor locations. (a) $(0{\cdot}9L_x, 0{\cdot}9L_y, 0{\cdot}9L_z)$; (b) $(0{\cdot}7L_x, 0{\cdot}7L_y, 0{\cdot}9L_z)$; (c) $(0{\cdot}5L_x, 0{\cdot}5L_y, 0{\cdot}9L_z)$; (d) $(0{\cdot}3L_x, 0{\cdot}3L_y, 0{\cdot}9L_z)$; (e) $(0{\cdot}1L_x, 0{\cdot}1L_y, 0{\cdot}9L_z)$: ——, potential energy control; — — —, squared pressure control; — — — —, energy density control. Secondary source at (L_x, L_y, L_z).

5. VISUALIZATION OF SOUND ATTENUATION

The evaluation of the total acoustic potential energy is insufficient to qualify the global effectiveness of the ANC due to the co-existence of multiple quiet zones and amplification zones. It also gives no idea on the locations of the quiet zones and the amplification zones as well as the degree of their effects in the enclosure. Therefore, the visualization of sound field inside the enclosed space is critical in analyzing the performance of ANC in a three-dimensional enclosed space.

In the present study, each dimension of the rectangular enclosure was divide into 21 grid points at which sound pressures under ANC will be calculated. The enclosure is thus define

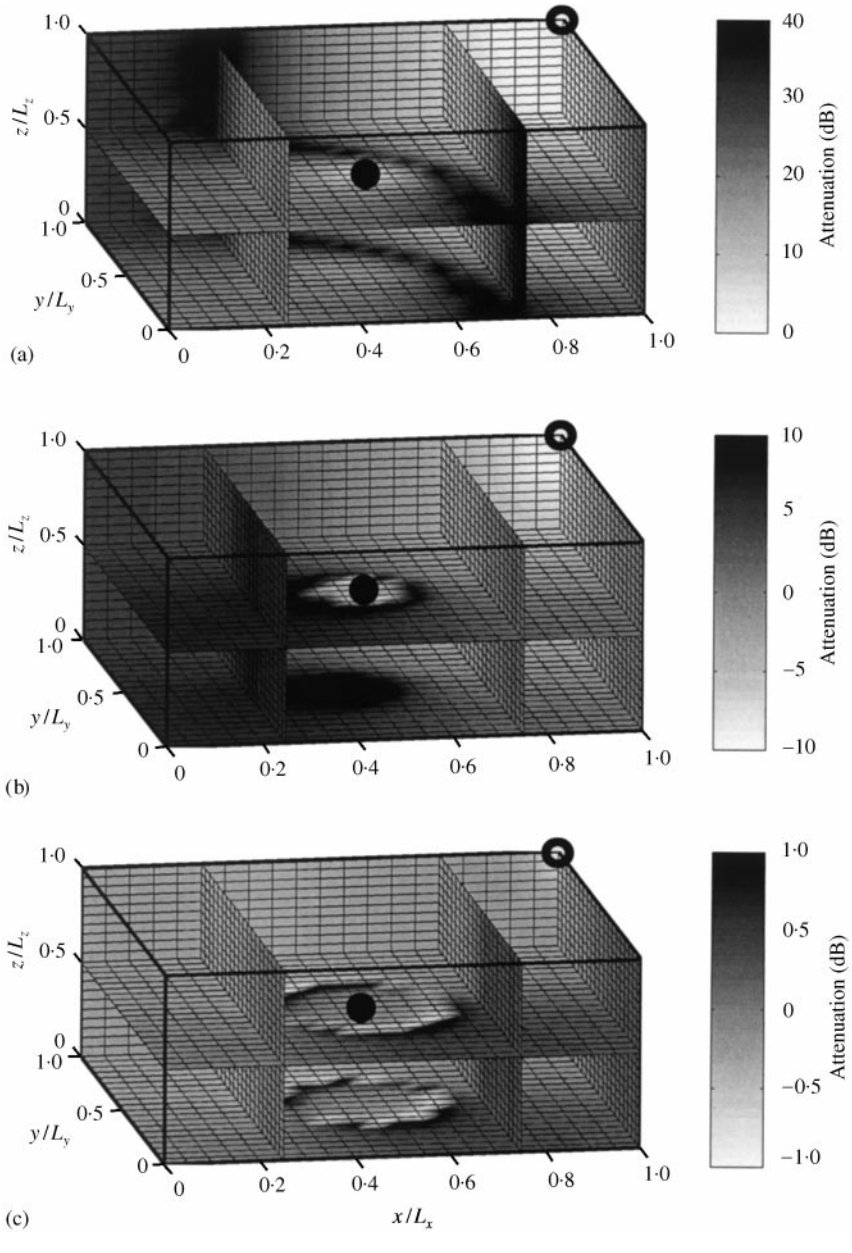

Figure 7. Attenuation of SPL under potential energy control for centre primary source: (a) $0{\cdot}3f_c$; (b) $0{\cdot}7f_c$; (c) $1{\cdot}1f_c$; (d) $1{\cdot}9f_c$; (e) $2f_c$; (f) $2{\cdot}9f_c$: ○, secondary source at (L_x, L_y, L_z); ●, primary sound source at $(0{\cdot}5L_x, 0{\cdot}5L_y, 0{\cdot}5L_z)$.

by 21 layers of 21×21 horizontal grid points. Attenuation of sound pressure level (SPL) was found from the difference between the calculated SPL before and after activating the secondary source. The secondary source S_s is fixed at the corner (L_x, L_y, L_z).

5.1. S_p AT ENCLOSURE CENTRE $(0{\cdot}5L_x, 0{\cdot}5L_y, 0{\cdot}5L_z)$

Figure 7(a) shows the SPL attenuation at $0{\cdot}3f_c$ inside the enclosed space under the potential energy control. A high global SPL attenuation is observed throughout the

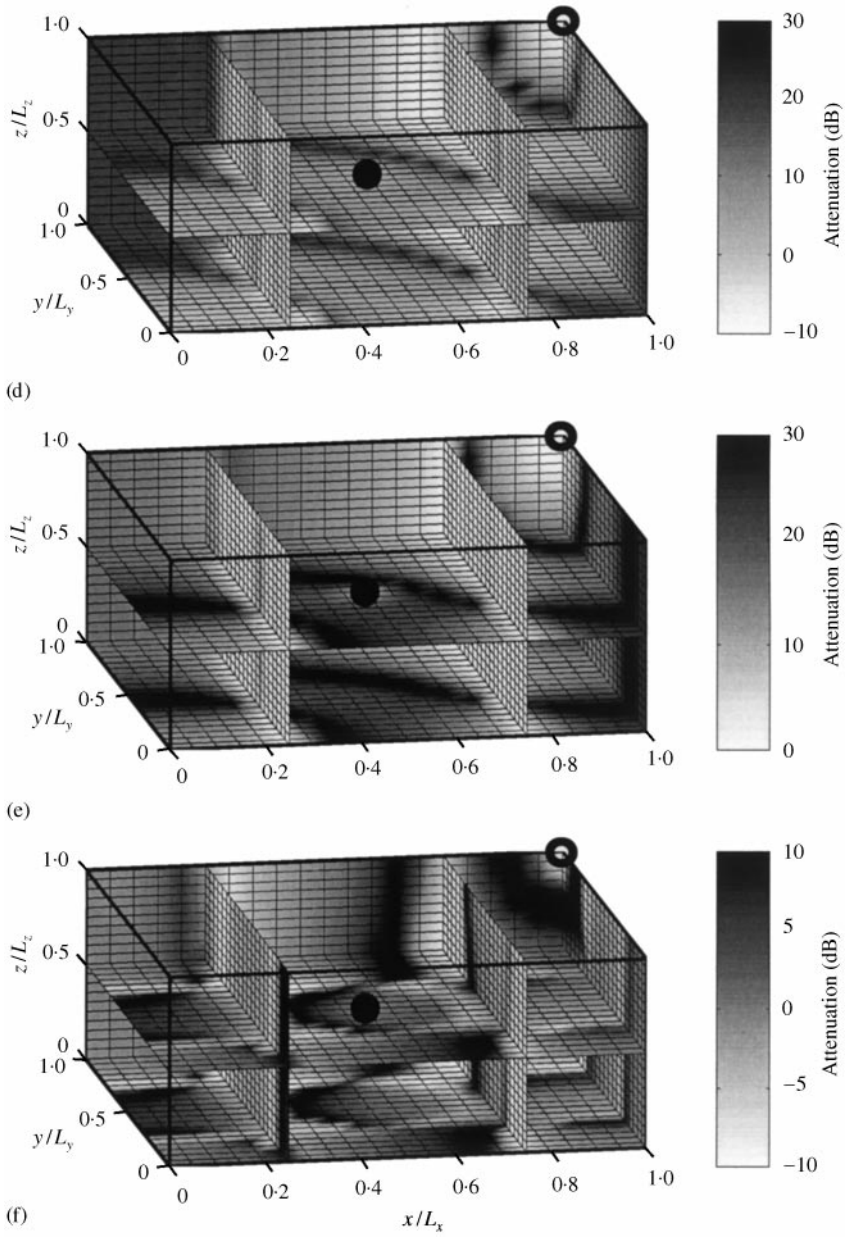

Figure 7. Continued.

enclosed space. The peak quiet zone occurs between the primary and secondary sources, and there is only little sound amplification at locations near to these sources. Even better global control can be observed at lower frequency. As frequency increases, the size of the quiet zone decreases. The high SPL attenuation region encloses the primary source and extends to the walls at $x/L_x = 0$ as shown in Figure 7(b) (at $0{\cdot}7f_c$). The sizes of the amplification zones near to the two sound sources increase as frequency increases towards f_c (Figures 7(a)–7(c)). It can also be observed from Figure 7(b) that the 10 dB zone of quiet can

only be found between a distance of $0{\cdot}1L_x$ and $0{\cdot}3L_x$ from the primary source at $0{\cdot}7f_c$. Within the frequency range from f_c to $1{\cdot}5f_c$, where the potential energy control algorithm cannot produce attenuation of the overall potential energy in the space as shown in Figure 3, the SPL attenuation is weak and the quiet zone becomes small. A typical example is given in Figure 7(c) (at $1{\cdot}1f_c$). The quiet zone disappears at f_c (not shown here). A strong quiet zone between the sources as in Figure 7(a) reappears at $1{\cdot}9f_c$ as shown in Figure 7(d). Figure 7(e) shows that the higher frequency, ANC can effectively control the sound field globally at frequencies close to that of the controllable eigenmode at $2f_c$ (Figure 3). Discrete quiet zones and amplification zones are found at higher frequencies (for instance, Figure 7(f) at $2{\cdot}9f_c$). It can be concluded from Figure 7 that under the potential energy control algorithm, the total potential energy is a good parameter to judge whether a global reduction of low-frequency sound can be achieved. However, since it is practically impossible to measure accurately this parameter, this control can hardly be implemented.

The squared-pressure control algorithm gives a good global noise control at very low frequency regardless of the location of the error sensor (not shown here). However, the SPL of the enclosed space is largely amplified at $0{\cdot}3f_c$ due to the detrimental effect as shown in Figure 8(a) except at the error sensor location ($0{\cdot}9L_x$, $0{\cdot}9L_y$, $0{\cdot}9L_z$) where a $\sim$280 dB SPL attenuation is found. The size of the quiet zone becomes far less than one-tenth of the acoustic wavelength. Also, the quiet zone at the location of error sensor becomes larger and sieges the secondary corner source as frequency increases towards f_c as shown in Figure 8(b). Though the squared-pressure control produces a quiet zone at a location near to the error sensor for a frequency between f_c and $2f_c$, the sound levels at other areas will be largely amplified. An example of this phenomenon is given in Figure 8(c), which shows the sound field at a frequency of $1{\cdot}5f_c$. The situation around $1{\cdot}7f_c$ is even worse (Figure 8(d)). It is probably due to the detrimental effect. It is not a spillover because the frequency $1{\cdot}7f_c$ is not at an eigenfrequency of the enclosure. A similar phenomenon also appears at frequencies close to $2f_c$, though both the amplitude and the areas of the sound amplification are reduced (Figure 8(e)). A relatively more uniform global attenuation of sound is achieved at $2f_c$ while the sound field pattern, except the magnitude, is very similar to that in Figure 8(e) and thus is not presented. As frequency increases, the quiet zones gradually shrink in size while the amplification zones gradually occupy regions opposite to the secondary sound source (Figure 8(f)). At even higher frequency, quiet zones reappear on the opposite side of the secondary source. The squared-pressure control then results in sound field patterns similar to those obtained under the potential energy control (cf. Figure 7(f)), except at or close to the frequencies at which the detrimental effect or spillover occurs (Figure 3). Therefore, they are not presented.

Both Figures 3 and 6, though they are related to different primary source locations, suggest that the detrimental effect below f_c can be removed when the error sensor is located at ($0{\cdot}1L_x$, $0{\cdot}1L_y$, $0{\cdot}9L_z$), which is a position opposite to the secondary source. With this error sensor location, global SPL attenuation with a large $\sim$40 dB quiet zone enclosing the error sensor can be achieved using the squared-pressure control algorithm at low frequency as shown in Figure 9(a). Again the quiet zone shrinks in size and the amplification zone appear as the frequency approaches f_c. A quiet zone is created around the secondary source as frequency increases beyond f_c. The sound field pattern at the frequency $1{\cdot}5f_c$ looks similar to that resulting when the error sensor is located close to the secondary source (Figure 9(b)). Global attenuation of sound is re-achieved at the frequency $2f_c$. Multiple quiet and amplification zones are found at higher frequencies as expected. Figure 9(c) shows an example for this at the frequency $2{\cdot}9f_c$.

Both Figures 8 and 9 suggest that a quiet zone can always be created near to the location of the error sensor. Also, a large attenuation of the total acoustic potential energy usually

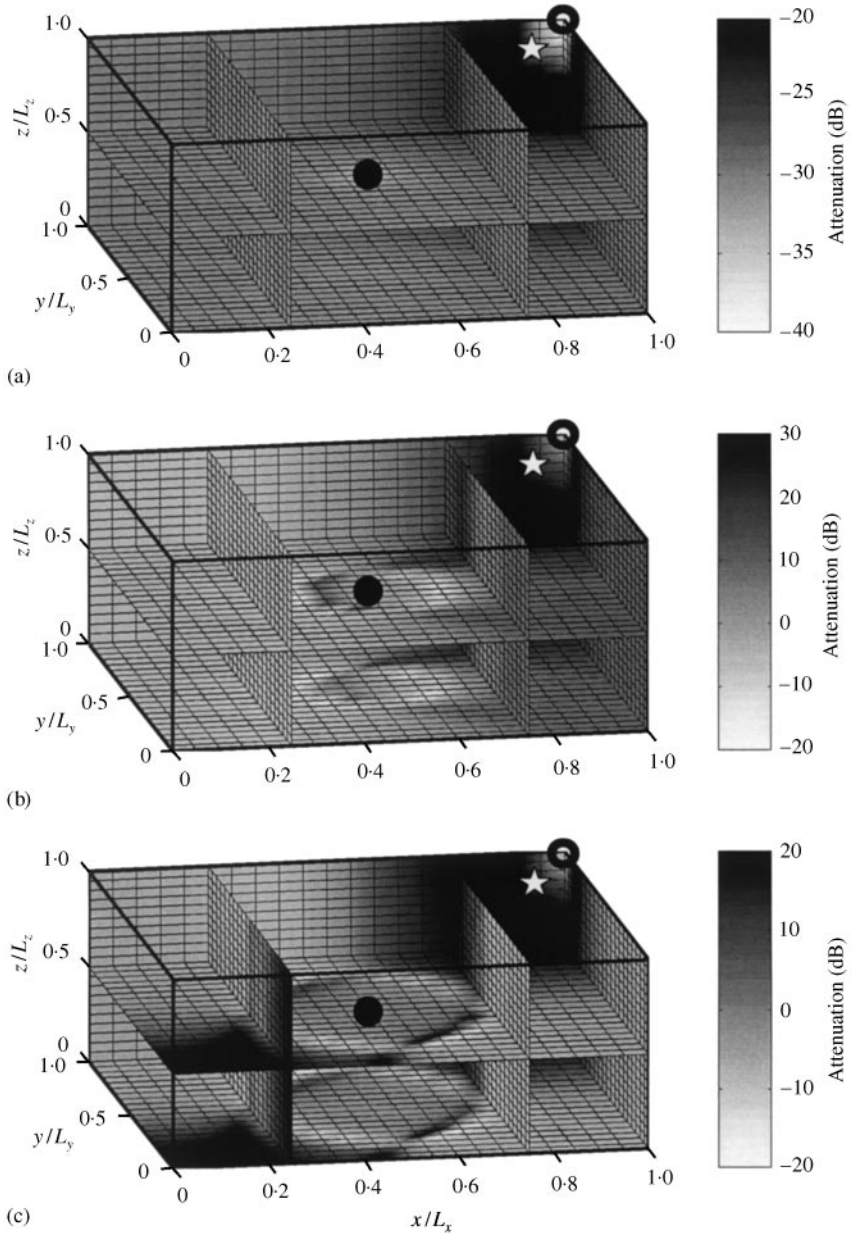

Figure 8. Attenuation of SPL under squared-pressure control for centre primary source: (a) $0{\cdot}3f_c$; (b) $0{\cdot}7f_c$; (c) $1{\cdot}5f_c$; (d) $1{\cdot}7f_c$; (e) $1{\cdot}9f_c$; (f) $2{\cdot}5f_c$: ○, secondary source at (L_x, L_y, L_z); ☆, error sensor at $(0{\cdot}9L_x, 0{\cdot}9L_y, 0{\cdot}9L_z)$; ●, primary sound source at $(0{\cdot}5L_x, 0{\cdot}5L_y, 0{\cdot}5L_z)$.

implies global sound attenuation. However, a complete global attenuation of sound cannot, in general, be achieved by using the squared-pressure control algorithm except at frequency much lower than f_c or at some eigenmode frequencies. Figure 8 and 9 manifest clearly a possibility of focussing attenuation at some walls or some parts inside the enclosure even at frequencies close to those of the detrimental effects and spillovers. This has a significant implication for building noise control.

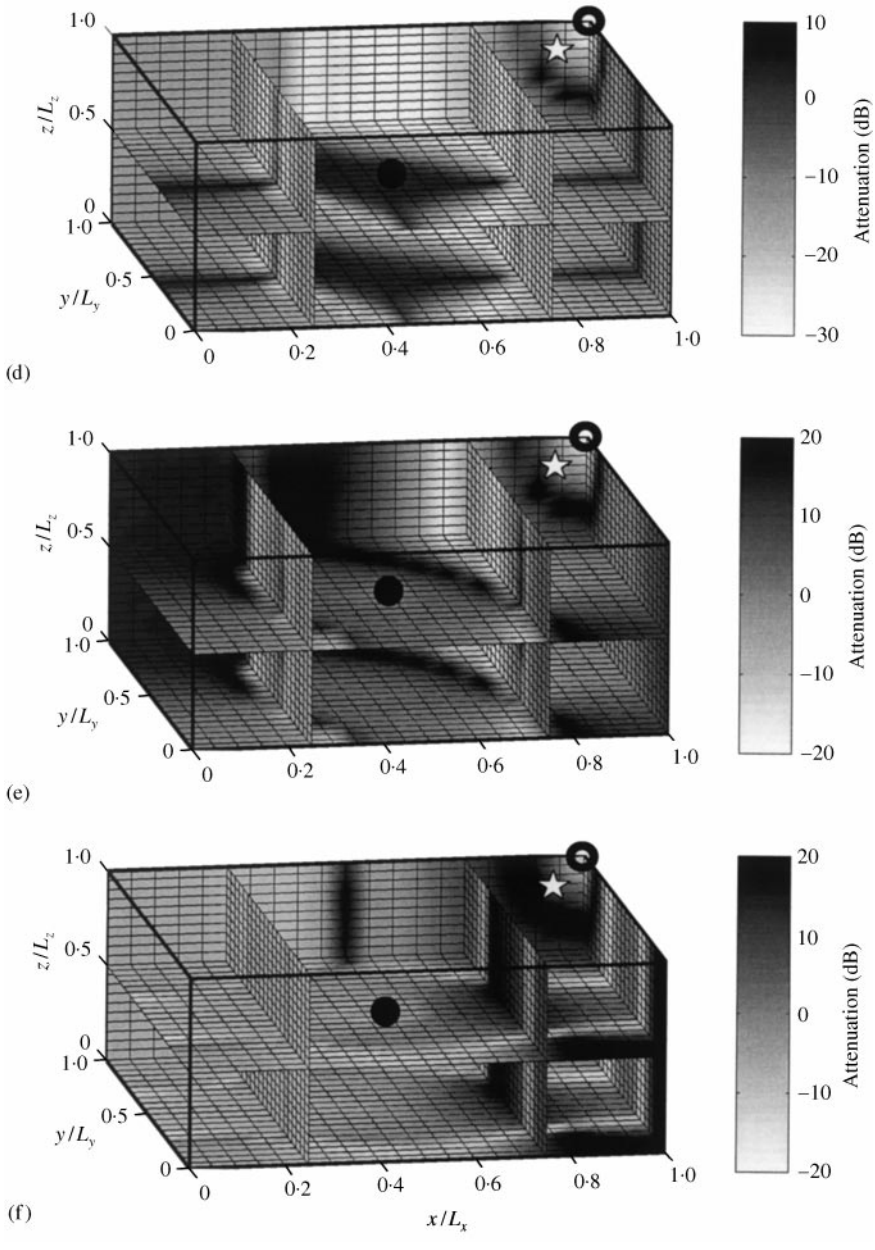

Figure 8. Continued.

Energy density control can eliminate many of the detrimental effects and spillovers as shown previously in Figures 3 and 6. For an error sensor near to the corner $(0{\cdot}9L_x, 0{\cdot}9L_y, 0{\cdot}9L_z)$, the attenuation of sound is not effective (maximum 3 dB variation within the enclosure). However, the energy density control does reduce the localized peak attenuation at the error sensor as well as the detrimental effects and spillovers, such as those at $0{\cdot}3f_c$ and $1{\cdot}7f_c$ respectively. Figure 10(a) shows a typical example at $1{\cdot}7f_c$. There is nearly no attenuation or amplification of SPL at $0{\cdot}3f_c$ and thus it is not presented here. This control algorithm avoids the creation of an undesirably large sound pressure gradient inside the

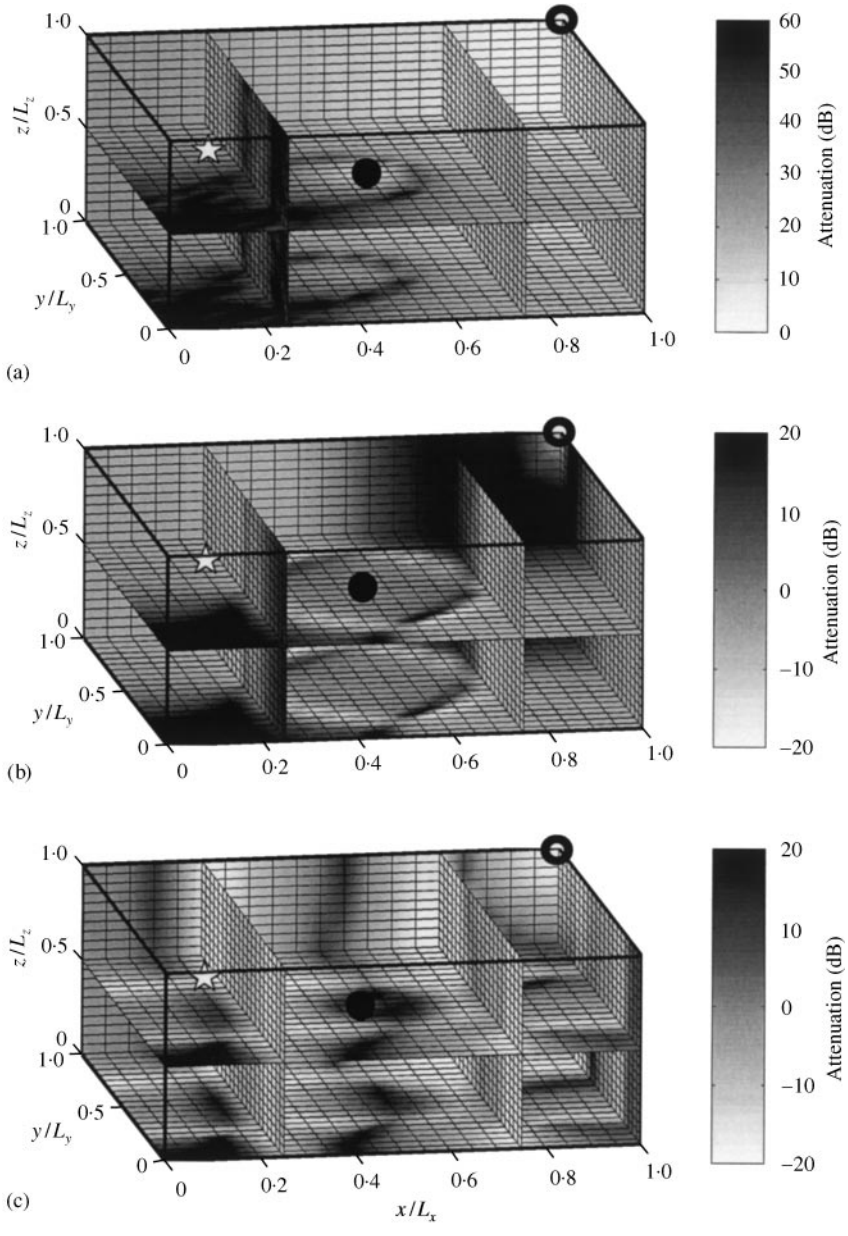

Figure 9. Attenuation of SPL under squared-pressure control for centre primary source: (a) $0{\cdot}3f_c$; (b) $1{\cdot}5f_c$; (c) $2{\cdot}9f_c$: ○, secondary source at (L_x, L_y, L_z); ☆, error sensor at $(0{\cdot}1L_x, 0{\cdot}1L_y, 0{\cdot}9L_z)$; ●, primary sound source at $(0{\cdot}5L_x, 0{\cdot}5L_y, 0{\cdot}5L_z)$.

enclosure. The corresponding sound fields for frequencies higher than f_c are similar to those under the squared-pressure control in patterns but not in magnitudes and in the standard deviations of the SPL attenuation among the 9253 points that define the space in this study (the source locations and six other points too near to the sources are excluded). The sound fields under the energy density control are more uniform. A typical example for this is given in Figure 10. The quiet zones become withered at increasing frequency as in the squared-pressure control cases (Figure 9(c)). Similar observations as in Figure 9 can be

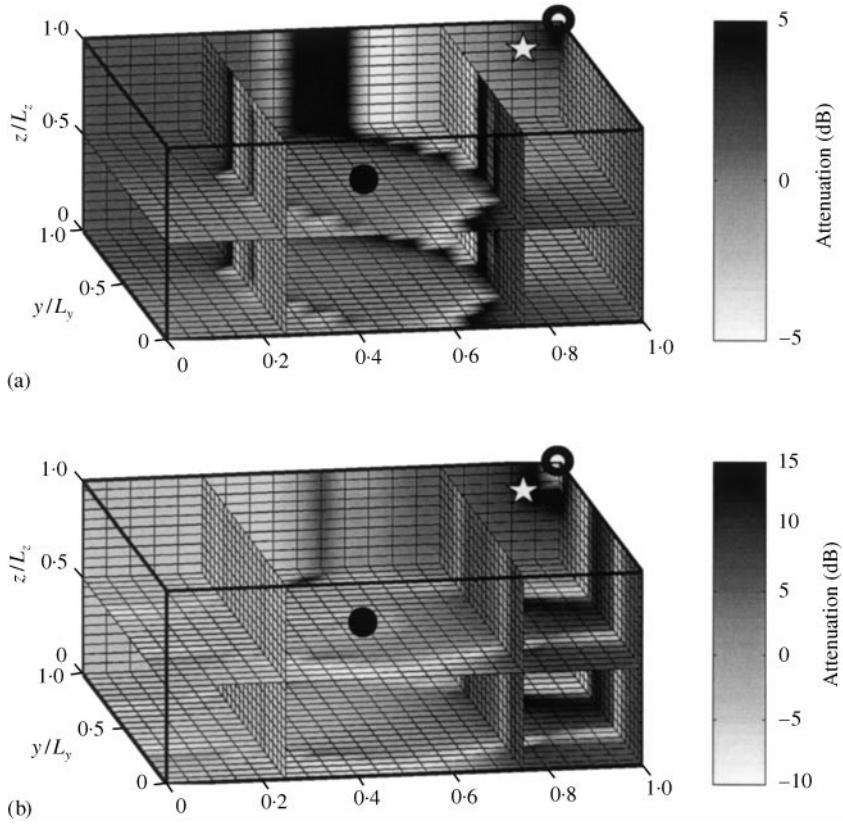

Figure 10. Attenuation of SPL under energy density control for centre primary source: (a) $1{\cdot}7f_c$; (b) $2{\cdot}5f_c$: ○, secondary source at (L_x, L_y, L_z); ☆, error sensor at $(0{\cdot}9L_x, 0{\cdot}9L_y, 0{\cdot}9L_z)$; ●, primary sound source at $(0{\cdot}5L_x, 0{\cdot}5L_y, 0{\cdot}5L_z)$.

made when the error sensor is located at the corner $(0{\cdot}1L_x, 0{\cdot}1L_y, 0{\cdot}9L_z)$. The advantage of using the energy density control is again in the more uniform resultant sound fields. Thus, they are not discussed.

It can be concluded here that the energy density control performs similarly to the squared-pressure one at frequencies other than those of the spillovers and detrimental effects. However, the energy density control can remove the detrimental effect observed in the squared-pressure case at low frequency. Also, since the energy density control can overcome these two disadvantages of the squared-pressure control with a reasonably higher possibility of achieving relatively more global reduction of sound level, it can be concluded that the former is a better algorithm for the present application.

5.2. OFFSET S_p AT $(0{\cdot}25L_x, 0{\cdot}5L_y, 0{\cdot}5L_z)$

It has been shown in the previous section that the energy density control is better than the squared-pressure control for implementing ANC in this slightly damped rectangular enclosed space. Therefore, this section is focused on the use of the former for controlling the sound field in the presence of an offset primary source.

Figure 11 shows the attenuation of sound field when the error sensor is located at the near corner $(0{\cdot}1L_x, 0{\cdot}1L_y, 0{\cdot}9L_z)$. At low frequency, the quiet zone is located behind the

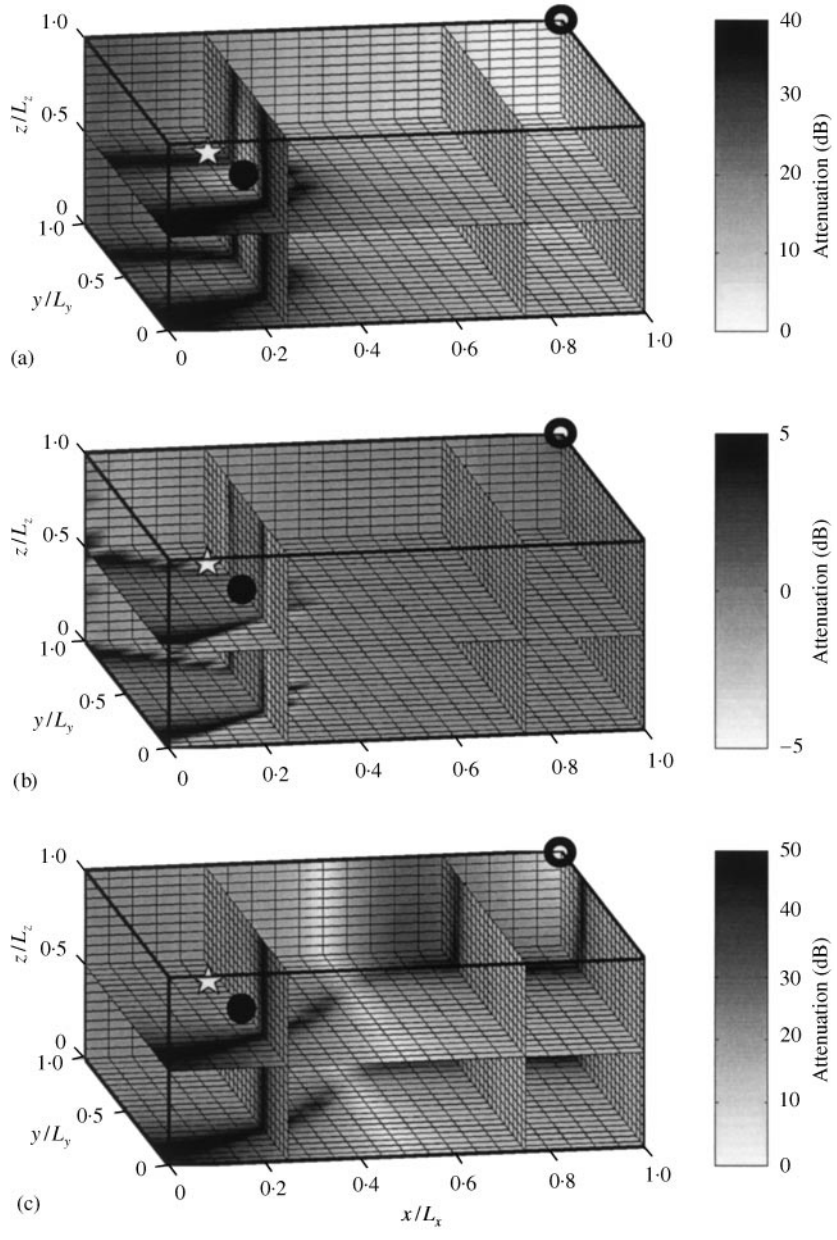

Figure 11. Attenuation of SPL under energy density control for offset primary source: (a) $0{\cdot}3f_c$; (b) $0{\cdot}7f_c$; (c) f_c; (d) $1{\cdot}5f_c$; (e) $1{\cdot}9f_c$; (f) $2{\cdot}5f_c$: ○, secondary source at (L_x, L_y, L_z); ☆, error sensor at ($0{\cdot}1L_x$, $0{\cdot}1L_y$, $0{\cdot}9L_z$); ●, primary sound source at ($0{\cdot}25L_x$, $0{\cdot}5L_y$, $0{\cdot}5L_z$).

primary source and it extends to the side and near walls (Figure 11(a)). Though some weak amplification of sound can be found around the strong quiet zone as frequency increases towards f_c, an approximately global SPL reduction can be achieved (Figure 11(b)). High sound attenuation can be achieved and a quiet zone appears around the secondary source at the frequency f_c (Figure 11(c)).

Sizes of the amplification zones increase with frequency but the quiet zone still exists on the walls near to the primary source (Figure 11(d)). The extension of quiet zone between the

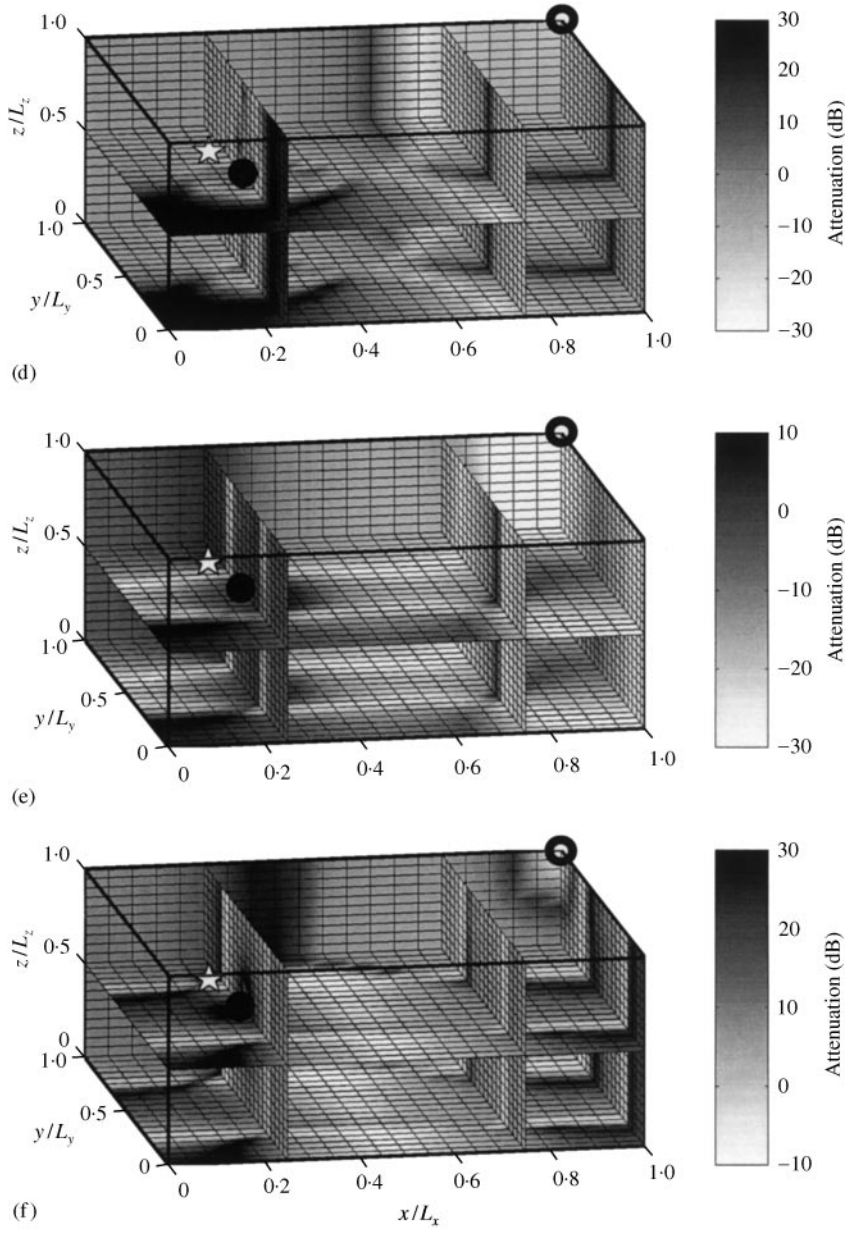

Figure 11. Continued.

primary source and the wall is probably due to the diffraction effect as suggested by Garcia-Bonito *et al.* [20]. At frequencies higher than $1{\cdot}5f_c$ and even within the amplification region of the total potential energy (Figure 6), SPL attenuation is still possible on the side walls and even on the near wall behind the primary source as shown in Figure 11(e). Unlike the case for the centre primary source, Figure 11(f) shows that the about 10 dB attenuation of the total acoustic potential energy at $2{\cdot}5f_c$ (Figure 6) does not imply global attenuation of sound.

ANC is again not effective when the error sensor is located near to the secondary source except at frequencies around f_c. However, the risk of large sound amplification resulting from the squared-pressure control can be reduced.

6. REMARKS

The present findings, though obtained from a simple ANC model consisting of a single secondary source, a single error sensor and a rectangular enclosure, show that ANC using the energy density sensing is very useful in building acoustics where the noise transmission out of a machine room is concerned. It is because the noise levels, especially those at low frequencies, on the major transmitting wall can be reduced effectively by this ANC. Though amplification of sound may be produced inside the enclosure, it is of secondary importance as there will seldom be people working for long hours inside the enclosure.

It should also be noted that complicated enclosure geometry is not favoured by practical building services and mechanical engineers for maintenance purpose and for the flexibility of space utilization. In noise control, the rectangular geometry enables an easy estimation of the room mode patterns and thus it will be easier for engineers to avoid the occurrence of the detrimental effect and the spillover. Also, complicated geometry will result in larger number of modal frequencies, nodal planes, etc., increasing the chance for the occurrence of the two above-mentioned adverse effects. This tends to make the control difficult to implement. The present findings on the performance of ANC under different cost functions should apply to any complicated enclosure geometry since the present analysis depends on knowledge of the room modes in principle. For complicated enclosure geometry, the room modes can be obtained using numerical methods. However, one should note that the squared-pressure control algorithm depends on the quality of the pressure signal, which is highly susceptible to the nodal planes or nodal points inside an enclosure. This is an inherited weakness of this type of algorithm, which is independent of the enclosure boundary.

Though global control of higher modal frequency and less amplification of sound pressure can be achieved with multiple secondary sources [16, 21], controlling high modal density with increasing number of secondary sources is not effective in practice [16]. Multiple error sensors can extend the size of the quiet zone only when the separations of sensors are much smaller than the required wavelength. Otherwise, small discrete quiet zones will be produced [22].

One should note that it is, in principle, only necessary to reduce the low-frequency sound level on the major sound-transmitting walls in a machine room in building noise control. The results of the present study illustrate that the possibility of producing large quiet zones on walls using one single energy density signal has its practical significance. Multiple sensing and sources may be useful in many situations, but they only increase the complexity of the ANC system, which can be satisfactorily implemented by a relatively simple configuration for the present purpose.

7. CONCLUSIONS

The effectiveness of a corner ANC system on the global control of sound inside a slightly damped rectangular enclosed space has been studied in the present study. The performance of three different control algorithms, namely the potential energy control, the squared-pressure control and the energy density control, is also investigated in terms of the

overall potential energy attenuation and resultant sound field patterns. The frequency range in the present study extends to three times the first cut-off frequency of the enclosure.

Basically, ANC is effective in creating a global reduction of sound level at low frequency. It is also effective at the eigenfrequencies unless the sources are located at the nodal planes of the corresponding eigenmodes. Besides, both quiet zones and amplification zones, which are the regions where attenuation and amplification of sound are found, respectively, are created as frequency increases beyond the first cut-off frequency of the enclosure. Potential energy control produces a quiet zone between the primary and secondary sources and has no effect at the above-mentioned uncontrollable eigenmode frequencies.

Detrimental effects have been observed under the squared-pressure control when error sensor is located near to a secondary corner source due to the small sound pressure created by this source at the error sensor position. These effects can be improved by increasing the separation between the error sensor and the secondary sound source so that the encountering of the former with the vanishing sound pressure points can be avoided. Also, spillovers occur at some uncontrollable modes. Under this control algorithm, regions of large amplification or attenuation of sound are created at different points inside the enclosure simultaneously. Sometimes, localized large sound attenuation with a relatively global sound amplification may result.

It is found that the energy density control is more effective if the error sensor and the corner secondary source are located on the two opposing sides of the primary source, so that the error sensor can obtain the energy density in a relatively uniform and representative region. This algorithm produces a more uniform sound field inside the enclosure than the squared-pressure control. The energy density control approach can also reduce the adverse impacts of both the detrimental effects and spillovers that appear under the squared-pressure control. Though the resultant sound fields under ANC with the squared-pressure and energy density control except at the frequencies of the detrimental effects and spillover are similar, the present results suggest that the energy density approach is better than the squared-pressure one in controlling sound in a slightly damped rectangular enclosure.

Though global reduction of sound level may not be achieved under ANC at all frequencies, the results obtained in the present study do show that there is a high possibility of producing significant sound attenuation at some areas on the boundaries of the enclosure using a simple configuration. This cannot be observed from total acoustic potential energy analysis. The detrimental effects for squared-pressure control and the ineffective energy density control due to small secondary source strength depend very much on the position of the error sensor. The present results are useful in the sound transmission control in buildings once the dominant frequency of the noise is known.

ACKNOWLEDGMENTS

The financial support from the Hong Kong Polytechnic University and the Research Grant Council, HKSAR Government is gratefully acknowledged.

REFERENCES

1. P. LUEG 1936 *U.S. Patent No.* 2 043 416. Process of silencing sound oscillations.
2. S. D. SOMMERFELDT, J. W. PARKINS and Y. C. PARK 1995 *Proceedings of ACTIVE* 95, *Newport Beach, CA, USA*, 477–488. Global active noise control in rectangular enclosures.
3. P. A. NELSON, A. R. D. CURTIS, S. J. ELLIOTT and A. J. BULLMORE 1987 *Journal of Sound and Vibration* **117**, 1–13. The active minimization of harmonic enclosed sound field. Part I: theory.

4. P. JOSEPH, S. J. ELLIOTT and P. A. NELSON 1993 *Journal of Sound and Vibration* **172**, 605–627. Near field zones of quiet.
5. J. GARCIA-BONITO, S. J. ELLIOTT and C. C. BOUCHER 1997 *Journal of the Acoustical Society of America* **101**, 3498–3516. Generation of zones of quiet using a virtual microphone arrangement.
6. S. J. ELLIOTT, P. JOSEPH, A. J. BULLMORE and P. A. NELSON 1988 *Journal of Sound and Vibration* **120**, 183–189. Active cancellation at a point in a pure tone diffuse sound field.
7. S. D. SOMMERFELDT, P. J. NASHIF 1994 *Journal of the Acoustical Society of America* **96**, 300–306. An adaptive filtered-x algorithm for energy-based active control.
8. Y. C. PARK and S. D. SOMMERFELDT 1997 *Journal of the Acoustical Society of America* **101**, 350–359. Global attenuation of broadband noise fields using energy density control.
9. X. QIU, C. H. HANSEN and X. LI 1998 *Journal of Sound and Vibration* **215**, 81–103. A comparison of near field acoustic error sensing strategies for the active control of harmonic free field sound radiation.
10. C. H. HANSEN and S. D. SNYDER 1997 *Active Control of Noise and Vibration*. London: E & FN Spon.
11. K. H. BAEK and S. J. ELLIOTT 1995 *Journal of Sound and Vibration* **186**, 245–267. Natural algorithms for choosing source locations in active control system.
12. S. S. RAO and T. S. PAN 1991 *American Institute of Aeronautics and Astronautics Journal* **29**, 942–943. Optimal placement of actuators in actively controlled structures using genetic algorithms.
13. G. S. CHEN, R. J. BRUNO and M. SALAMA 1991 *American Institute of Aeronautics and Astronautics Journal* **29**, 1327–1334. Optimal placement of active/passive members in truss structures using simulated annealing.
14. S. D. SNYDER and C. H. HANSEN 1991 *Journal of Sound and Vibration* **148**, 537–542. Using multiple regression to optimize active noise control system design.
15. S. D. SNYDER and C. H. HANSEN 1994 *Journal of Sound and Vibration* **170**, 433–449. The design of systems to actively control periodic sound transmission into enclosed spaces. Part 1. Analytical models.
16. P. A. NELSON and S. J. ELLIOTT 1992 *Active Control of Sound*. London: Academic Press.
17. D. Y. MAA 1994 *Applied Acoustics* **41**, 113–126. Sound field in a room and its active noise control.
18. P. JOSEPH, S. J. ELLIOTT and P. A. NELSON 1994 *Journal of Sound and Vibration* **172**, 629–655. Statistical aspects of active control in harmonic enclosed sound fields.
19. A. J. BULLOMRE, P. A. NELSON, A. R. D. CURTIS and S. J. ELLIOTT 1987 *Journal of Sound and Vibration* **117**, 15–33. The active minimization of harmonic enclosed sound field. Part II: computer simulation.
20. J. GARCIA-BONITO, S. J. ELLIOTT and M. BONILHA 1997 *Journal of Sound and Vibration* **201**, 43–65. Active cancellation of pressure at a point in a pure tone diffracted diffuse sound field.
21. M. MIYOSHI and Y. KANEDA 1991 *Noise Control Engineering Journal* **36**, 85–90. Active control of broadband random noise in a reverberant three-dimensional space.
22. S. J. ELLIOTT and J. GARCIA-BONITO 1995 *Journal of Sound and Vibration* **186**, 696–704. Active cancellation of pressure and pressure gradient in a diffuse sound field.